Towards a better understanding of the parameters determining the competition between bromine halogen bonding and hydrogen bonding : an FTIR spectroscopic study of the complexes between bromodifluoromethane and trimethylamine

Towards a better understanding of the parameters determining the competition between bromine halogen bonding and hydrogen bonding: an FTIR spectroscopic study of the complexes between bromodifluoromethane and trimethylamine.

Yannick Geboes[a,b], Frank De Proft[b] and Wouter A. Herrebout[a]*

[a] *Department of Chemistry, University of Antwerp, Groenenborgerlaan 171, 2020 Antwerp (Belgium), E-mail: Wouter.herrebout@uantwerpen.be*

[b] *Eenheid Algemene Chemie (ALGC), Member of the QCMM VUB-UGent Alliance Research Group, Vrije Universiteit Brussel (VUB), Pleinlaan 2, 1050 Brussels (Belgium)*

Corresponding Author:

W.A. Herrebout: e-mail: wouter.herrebout@uantwerpen.be, +32/3.265.33.73

Keywords: noncovalent interactions, halogen bonding, hydrogen bonding, FTIR, cryospectroscopy

Abstract

Previous experimental and theoretical studies of various model compounds dissolved in liquid noble gases have shown that iodine halogen bonding can compete with hydrogen bonding and that experimental information on the thermodynamic equilibria present can be derived. To get a more general grasp of the competition between halogen bonding and hydrogen bonding, and to expand the set of experimental data to other, weaker, halogen donors, solutions in liquid krypton containing mixtures of bromodifluoromethane with trimethylamine or the fully deuterated trimethylamine-d_9 are studied using FTIR spectroscopy. Analysis of the experimental data obtained is supported by *ab initio* calculations, statistical thermodynamics and Monte Carlo-Free Energy Perturbation calculations. Careful comparison of the spectra of the monomers and of the mixtures studied, shows that for all solutions studied, only features due to a hydrogen-bonded complex are observed. The experimental complexation enthalpy for this species is determined to be -14.2(4) kJ mol^{-1}.

1. Introduction

Halogen bonding (XB), the noncovalent interaction in which covalently bonded halogen atoms interact with electron rich moieties through a region with positive electrostatic potential along the covalent bond axis, the σ-hole, has been widely studied in the past decades. [1-4] Within these studies, it was found that the strength of the noncovalent interactions correlates well with the size of the σ-hole on the halogen atom involved. [5] Ways to increase the size of the σ-hole, and thus strengthen the noncovalent interactions formed include enhancing the electron withdrawing properties of the covalently bonded molecule [6] and increasing the size of the halogen atom involved. [7] Another aspect relevant to the field of halogen bonding is its relationship with the more ubiquitous hydrogen bonds (HB). [8] It has been demonstrated that these noncovalent interactions are able to coexist, [9-11] cooperate [12] and compete [13-17] with each other in several theoretical and experimental studies.

In previous studies, we have investigated the competition between iodine halogen bonding and hydrogen bonding by performing infrared and Raman measurements on liquid noble gas solutions containing one of several Lewis bases and the combined donor molecules difluoroiodomethane (CHF_2I) [18-19] or fluoroiodomethane (CH_2FI) [20]. The experimental measurements, performed at thermodynamic equilibrium, were supported by *ab initio* calculations to assign the complex bands observed and rationalize the results. In these studies, it was demonstrated that softer Lewis bases tend to prefer iodine halogen bonding over hydrogen bonding, while decreasing the number of fluorine atoms on the donor molecule weakens both noncovalent interactions.

As the size of the halogen atom involved is one of the key factors determining the strength of the halogen bond formed, we wish to investigate the effect of using a bromine atom (instead of an iodine atom) as a halogen bond donor on the competition with hydrogen bonding. Therefore, in the current study, the complexes formed between bromodifluoromethane (CHF_2Br) and trimethylamine (TMA) in liquid krypton (LKr) solutions are studied using FTIR. The choice for CHF_2Br is motivated by the fact that the use of a small molecule avoids complications in the spectra associated with internal rotations, while the presence of two fluorine atoms enhances the strength of the noncovalent interactions formed. Since it was shown in a previous study [18] that for the combination of CHF_2I with TMA the halogen-bonded complex is significantly more stable than the hydrogen-bonded complex, the same Lewis base is used within this study to give the halogen-bonded complex the best possible chance to compete with its hydrogen-bonded counterpart.

The results obtained within this study will be compared with the results of previous studies involving TMA with CHF_2I to assess how substituting the iodine atom with a bromine atom influences the strength of both noncovalent interactions. Furthermore, an additional comparison with the results for the complex between fluoroform (CF_3H) and TMA will yield information on the influence of the third

halogen atom of a CHF_2X (X = F, Br, I) molecule on the formed hydrogen bond. To reveal the effect of adding fluorine atoms to the covalently bonded molecule on halogen bonding, the results are also compared with those of the halogen-bonded complex between TMA and bromotrifluoromethane (CF_3Br).

2. Experimental

Bromodifluoromethane (CHF_2Br) was purchased from Fluorochem and was used without further purification. Trimethylamine (TMA, 99%) and fully deuterated trimethylamine (TMA-d_9, +99% d) were purchased from Sigma-Aldrich and were used without further purification. The solvent gas krypton was supplied by Air Liquide and had a stated purity of 99.9995%. When referring to (measurements or results of) both undeuterated and fully deuterated the notation TMA(-d_9) is used in the remainder of this paper.

The infrared spectra were recorded on a Bruker 66v FTIR spectrometer, equipped with a globar source, a Ge/KBr beam splitter and MCT detector, cooled with liquid nitrogen. Measurements were conducted in cells equipped with Si windows and a path length of 10 mm [21] to obtain spectra between 6500 cm^{-1} and 450 cm^{-1}. All interferograms were averaged over 500 scans, Blackman-Harris 3-term apodized and Fourier transformed with a zero filling factor of 8 to yield spectra with a resolution of 0.5 cm^{-1}.

Estimated mole fractions of the solutions varied between 1.3×10^{-4} and 2.3×10^{-3} for CHF_2Br and 5.6×10^{-4} and 1.5×10^{-3} for TMA(-d_9). As the experimental setup does not allow for verification of full solubility of the compounds, or verification of the fluid level in the filling tube, exact concentrations are not known. The monomers CHF_2Br and TMA and the complexes formed are believed to be fully soluble in LKr in both the concentration and the temperature ranges studied, as no traces of crystallization or changes due to a decrease or increase in solubility were observed during any of the measurements.

Experimental complexation enthalpies were determined from van ‘t Hoff plots, based on measurements performed in the 120-156 K temperature interval. The concentrations of the different solutions studied, and the temperature intervals used are summarized in the ESI. Using a subtraction procedure in which spectra of monomer solutions, recorded at identical temperatures and similar concentrations, are rescaled and subtracted from the spectrum of the mixture, spectra are obtained containing solely complex bands, [21] The corresponding band intensities for monomers and complexes are obtained using numerical integration. Thermal expansion of the solvent gas during temperature studies was accounted for using the method published by van der Veken [22]. To ensure that no

numerical instabilities due to the non-linearity of the MCT detector used could occur during analysis, for all numerical procedures performed, only complex and monomer with an absorbance below 1.0 were considered.

To support our experimental measurements, *ab initio* MP2 calculations were performed using Dunning's augmented correlation consistent basis set of double zeta quality (aug-cc-pVDZ) in Gaussian09. [23] The standard aug-cc-pVDZ basis set was used for hydrogen, carbon, nitrogen, fluorine and chlorine, while aug-cc-pVDZ-PP basis set including a small-core energy-consistent relativistic pseudopotential (PP) was used for bromine. [24-25] The counterpoise technique as proposed by Boys and Bernardi [26] was used during all *ab initio* calculations to account for basis set superposition error. Energies at the basis set limit were calculated with Molpro [27] using the extrapolation scheme of Truhlar [28] in which the effect of electron correlation is obtained from MP2 calculations.

$$E_{CBS}^{HF} = \frac{3^{\alpha}}{3^{\alpha} - 2^{\alpha}} E_3^{HF} - \frac{2^{\alpha}}{3^{\alpha} - 2^{\alpha}} E_2^{HF} \quad (1)$$

$$E_{CBS}^{cor,MP2} = \frac{3^{\beta}}{3^{\beta} - 2^{\beta}} E_3^{cor,MP2} - \frac{2^{\beta}}{3^{\beta} - 2^{\beta}} E_2^{cor,MP2} \quad (2)$$

In these calculations α = 3.4 and β=2.2, [28] while energies with subscript 2 and 3 are calculated using the aug-cc-pVDZ(-PP) and aug-cc-pVTZ(-PP) basis sets respectively.

Furthermore, a correction for higher order correlation effects is made using the method of Jurečka and Hobza [29], yielding results of $E_{CBS}^{CCSD(T)}$ quality.

$$\Delta E^{CCSD(T)} = \left| E^{CCSD(T)} - E^{MP2} \right|_{aug-cc-pVDZ(-PP)} \quad (3)$$

$$E_{CBS}^{CCSD(T)} = E_{CBS}^{HF} + E_{CBS}^{cor,MP2} + \Delta E^{CCSD(T)} \quad (4)$$

Complexation enthalpies in the vapor phase ΔH°(vap,calc) were obtained from the calculated complexation energies ΔE(CCSD(T)) by applying a zero-point energy correction and a correction for thermal effects, calculated at the MP2/aug-cc-pVDZ(-PP) level of theory. Correction of these calculated enthalpy values with solvent effects yields complexation enthalpies in liquid krypton (LKr) ΔH°(LKr,calc) which can be compared with the experimental complexation enthalpies ΔH°(LKr). Corrections for thermal effects and zero-point vibrational contributions were obtained using statistical thermodynamics, whereas effects of solvation were accounted for using the Monte Carlo Free Energy Perturbation (MC-FEP) approach as implemented in an in-house modified version of BOSS 4.0. [30]

3. Results

3.1. *Ab initio* calculations

Two stable complex geometries were obtained from *ab initio* calculations at the MP2/aug-cc-pVDZ-PP level for the CHF_2Br·TMA dimer. In the first complex, CHF_2Br interacts through its bromine atom

with the nitrogen atom in TMA, thus forming a halogen-bonded complex, while in the second dimer the hydrogen atom of CHF_2Br interacts with the nitrogen atom, forming a hydrogen-bonded complex. Both equilibrium geometries have a C_s symmetry and are shown in Figure 1. The main intermolecular structural parameters and relative energies are summarized in Table 1. Cartesian coordinates of both monomers and complexes are given in Tables S1 and S2 of the ESI.

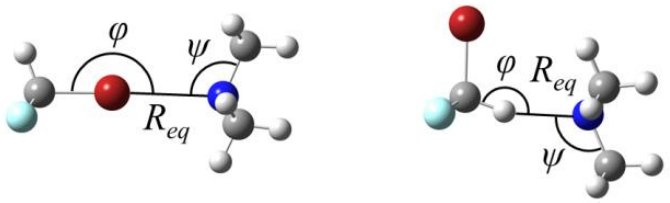

Figure 1: *Ab initio* calculated MP2/aug-cc-pVDZ-PP geometries for the halogen-bonded (left) and hydrogen-bonded complex (right) of CHF_2Br with TMA.

Table 1: Intermolecular distance R_{eq} (Å), bond angles (°), MP2/aug-cc-pVDZ-PP ΔE(DZ) and CCSD(T)/CBS ΔE(CCSD(T)) extrapolated complexation energies, calculated vapor phase complexation enthalpies Δ*H*° (vap,calc), the calculated complexation enthalpies in liquid krypton (Δ*H*° (LKr,calc)) and the corresponding experimentally obtained complexation enthalpies (Δ*H*° (LKr)) (kJ mol^{-1}) for the complexes of CHF_2Br with TMA. For comparison, the Δ*H*° (LKr,calc) and (Δ*H*° (LKr) values for the CHF_2I·TMA complexes are also included (kJ mol^{-1}).

	CHF_2Br	
	XB	HB
$R_{eq}=R_{X\cdots N}$ [a]	2.94	2.22
$\varphi_{C\text{-}X\cdots N}$ [a]	178.4	162.3
$\psi_{C\text{-}N\cdots X}$ [a]	111.8/107.1/107.1	115.5/105.8/105.8
Δ*E* (DZ)	-19.0	-23.8
Δ*E* (CCSD(T))	-19.1	-24.8
Δ*H*° (vap,calc)	-16.7	-22.0
Δ*H*° (LKr,calc)	-13.6	-16.5
Experimental		
Δ*H*° (LKr)	-	-14.2(4)
Δ*H*° (CHF_2I, LKr,calc) [b]	-23.4	-16.6
Δ*H*° (CHF_2I , LKr) [c]	-19.0(3)	-14.7(2)

[a] X = Br (in XB), H (in HB)
[b] values calculated using identical parameters, reported by Geboes et al. [20]
[c] values reported by Nagels et al. [18]

For the halogen-bonded complex between CHF_2Br and TMA a nearly linear geometry is found (φ = 178.43°), while for the hydrogen-bonded complex the C-H···N angle φ decreases to 162.3°. As before for the complexes formed with difluoroiodomethane, [18-19] this deviation from a linear geometry can be

explained by the ability to form secondary interactions in the hydrogen-bonded complex, which have been revealed by the noncovalent interactions (NCI) index visualized using NCIPLOT [31-32]. Plots of the reduced density gradient versus the electron density multiplied by the sign of the second Hessian eigenvalue and figures showing the gradient isosurfaces are given in Figure 2. Indeed, for the halogen-bonded complex a single disk-like surface is observed between bromine and the nitrogen atom, whereas for the hydrogen-bonded complex, apart from the disk-like surface between hydrogen and nitrogen, a broad surface is observed between the diffuse bromine atom and hydrogen atoms of two of the methyl groups of TMA.

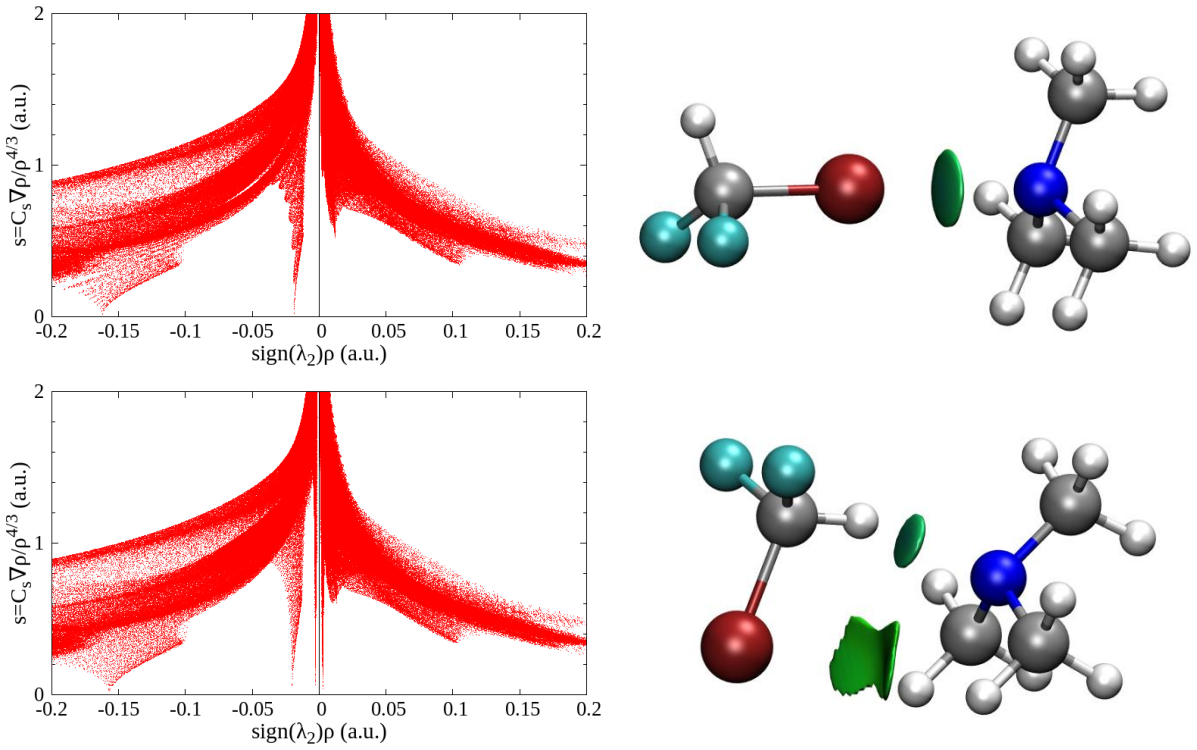

Figure 2: Plots of the reduced density gradient versus the electron density multiplied by the sign of the second Hessian eigenvalue (left) and gradient isosurfaces (s = 0.5 a.u., right) for the halogen-bonded complex (top) and the hydrogen-bonded complex (bottom) between CHF_2Br and TMA.

3.2 Infrared spectroscopy

An overview of experimentally observed monomer bands, complexation shifts and the corresponding calculated shifts is given in Table 2 for TMA and Table 3 for TMA-d_9. A selection of the spectral regions discussed in this study is given in Figure 3 for CHF_2Br·TMA mixtures and Figure 4 for CHF_2Br·TMA-d_9 mixtures.

The assignments of the experimental frequencies of TMA and TMA-d_9 are based on previous studies, whereas the assignment of the CHF_2Br bands and complex bands is based on *ab initio* calculations at

the MP2/aug-cc-pVDZ-PP level of theory, for which the results are given in Tables S3 and S4 of the ESI.

3.2.1 CH_2FBr·TMA infrared spectra

Investigation of the subtracted spectra of the mixtures of bromodifluoromethane (CHF_2Br) with TMA reveals clear complex bands in several spectral regions. To assess whether these bands can be assigned to halogen or hydrogen-bonded complex, spectral regions where both complex isomers have opposing shifts are the first focus of this study. One such region is found for the CHF_2Br ν_4 spectral region, shown in panel 3C, for which a redshift of -8.0 cm^{-1} is calculated for the hydrogen-bonded complex and a blueshift of 0.2 cm^{-1} for the halogen-bonded complex. Upon subtraction, using a subtraction factor for CHF_2Br determined in another spectral region, only a -8.2 cm^{-1} redshifted band corresponding to the hydrogen-bonded complex is retained. For the CHF_2Br ν_2 vibrational mode a 43.0 cm^{-1} blueshifted band is predicted for the hydrogen-bonded complex, while a -0.3 cm^{-1} redshift has been calculated for the halogen-bonded complex. Upon subtraction, a large 32.3 cm^{-1} blueshifted band is retained, as can be seen in panel B of Figure 3, which is assigned to the hydrogen-bonded complex. The second complex band in this panel at 1268 cm^{-1} is assigned to the ν_{18} mode of TMA, for which experimental shift of -5.1 cm^{-1} corresponds well to the calculated value of -4.9 cm^{-1} for the hydrogen-bonded complex. Finally, the absence of halogen-bonded complex can also be observed in the CHF_2Br ν_7 spectral region, shown in panel 3A, where a 33.5 cm^{-1} blueshifted band is observed corresponding to the hydrogen-bonded complex with a calculated shift of 59.9 cm^{-1}. On the right-hand side of this panel, the more intense hydrogen-bonded complex band of the ν_2 mode of CHF_2Br can also be seen in part, but no complex band corresponding to the halogen-bonded complex, for which a redshift of -2.5 cm^{-1} is calculated, is observed in the spectra.

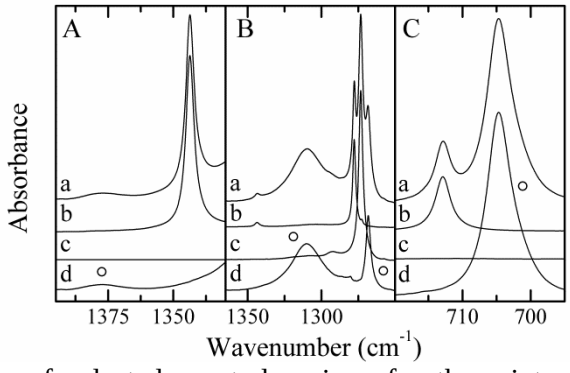

Figure 3: Infrared spectra of selected spectral regions for the mixtures of CHF_2Br with TMA dissolved in LKr at 120 K. In each panel, trace *a* represents the mixed solution, while traces *b* and *c* show the rescaled spectra of the solutions containing only CHF_2Br or TMA, respectively. Trace *d* represents the spectrum of the complex which is obtained by subtracting the rescaled traces *b* and *c* from trace *a*. Bands due to the hydrogen-bonded complex observed in traces *d* are marked with an open circle (°). Estimated mole fractions of the solutions of the mixtures are 2.3×10^{-3} for CHF_2Br and 5.6×10^{-4} for TMA-d_9 in panel A, 3.8×10^{-4} for CHF_2Br and 7.5×10^{-4} for TMA-d_9 in panel B and C.

Table 2: Experimental vibrational frequencies for the monomers and complex, experimental complexation shifts ($\Delta\nu_{exp,HB}$) and MP2/aug-cc-pVDZ-PP calculated complexation shifts, in cm^{-1}, for the hydrogen-bonded complex ($\Delta\nu_{calc,HB}$) and halogen-bonded complex ($\Delta\nu_{calc,XB}$) of CHF_2Br with TMA dissolved in LKr at 120 K.

	Assignment	$\nu_{monomer}$	$\nu_{complex}$	$\Delta\nu_{exp,HB}$	$\Delta\nu_{calc,HB}$	$\Delta\nu_{calc,XB}$
CHF_2Br		3025.4	-			
	ν_1	3014.4	[a]		-74.1	-12.1
	ν_7	1343.6	1377.1	33.5	59.9	-2.5
	ν_2	1277.8	1310.1	32.3	43.0	-0.3
	ν_8	1119.7	1107.5	-12.2	-12.3	-19.3
	ν_3	1093.5	1080.9	-12.6	-13.1	-6.7
	ν_4	712.9	704.7	-8.2	-8.0	0.2
	ν_5	578.0	576.8	-1.2	-0.8	-4.9
TMA	ν_{12}	2977.0	2980.8	3.8	1.2	0.1
	ν_1	2944.4	2947.5	3.1	3.0	1.6
	ν_{13}	2944.4	2947.5	3.1	3.3	1.5
	$2\,\nu_4$	2818.6	2821.9	3.3	2.9	0.9
	ν_2	2769.0	2778.2	9.2	16.9	12.4
	ν_{14}	2769.0	2778.2	9.2	19.3	13.7
	$\nu_{20}+\nu_{21}$	1474.8	1472.5	-2.3	-6.4	-2.7
	ν_{15}	1467.6	1469.6	2.0	1.4	0.1
	ν_3	1454.8	1453.8	-1.0	2.0	-0.4
	ν_4	1438.8	1440.6	1.8	1.4	0.4
	ν_{16}	1438.8	1440.6	1.8	1.0	-1.1
	ν_{17}	1405.3	-		1.5	0.4
	ν_{18}	1273.3	1268.2	-5.1	-4.9	0.0
	ν_5	1184.3	1192.9	8.6	8.4	5.0
	ν_{19}	1098.5	1099.3	0.8	-0.5	-1.3
	ν_{20}	1041.5	1036.3	-5.2	-4.2	-1.2
	ν_6	828.1	826.2	-1.9	-3.9	-3.5

[a] Band could not be assigned due to overlap with TMA C-H stretching modes.

3.2.2 CH_2FBr·TMA-d_9 infrared spectra

In addition to the spectral regions discussed for mixtures with TMA, the use of TMA-d_9 also enables the inspection of the C-H stretching mode of CHF_2Br. For this CHF_2Br ν_1 spectral region, shown in panel A of Figure 4, a complex band with a redshift of -42.7 cm^{-1} is observed, corresponding to the hydrogen-bonded complex with a calculated shift of -74.3 cm^{-1}. No second redshifted band, corresponding to the predicted redshift of -12.1 cm^{-1} for the hydrogen-bonded complex is observed. For the other three spectral regions discussed for the CHF_2Br·TMA mixtures, analogous results were obtained, confirming the absence of halogen-bonded complex. These spectral regions are also shown in Figure 4, while an overview of the experimental and calculated shifts is given in Table 3.

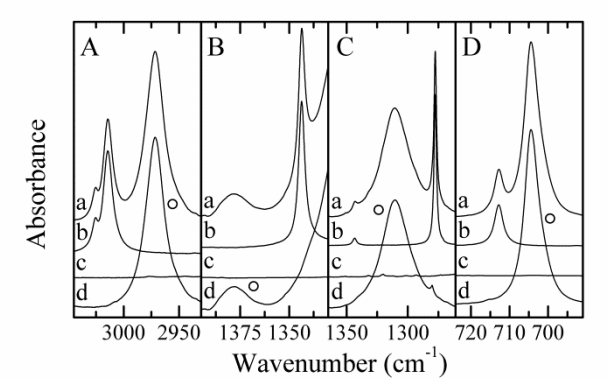

Figure 4: Infrared spectra of selected spectral regions for the mixtures of CHF_2Br with TMA-d_9 dissolved in LKr at 120 K. In each panel, trace *a* represents the mixed solution, while traces *b* and *c* show the rescaled spectra of the solutions containing only CHF_2Br or TMA-d_9, respectively. Trace *d* represents the spectrum of the complex which is obtained by subtracting the rescaled traces *b* and *c* from trace *a*. Bands due to the hydrogen-bonded complex observed in traces *d* are marked with an open circle (°). Estimated mole fractions of the solutions of the mixtures are 2.3×10^{-3} for CHF_2Br and 5.6×10^{-4} for TMA-d_9 in panel A, 2.3×10^{-3} for CHF_2Br and 1.5×10^{-3} for TMA-d_9 in panel B and 3.8×10^{-4} for CHF_2Br and 7.5×10^{-4} for TMA-d_9 in panels C and D.

Just as in the previous study of the $CH_2FI{\cdot}TMA(\text{-}d_9)$ complexes, [20] a complex band for the ν_3 mode of TMA-d_9 is observed in the infrared spectrum, despite the fact that this mode has too low an intensity to be observed for the monomer, as shown in Figure 5. As shown in Table S4B of the ESI, upon complexation, the calculated infrared intensity rises from 0.2 km mol^{-1} for the monomer to 1.3 km mol^{-1} for the hydrogen-bonded complex. To determine the experimental complexation shift, the vibrational frequency of the monomer is determined using Raman spectroscopy in LKr at the same temperature as the FTIR measurements.

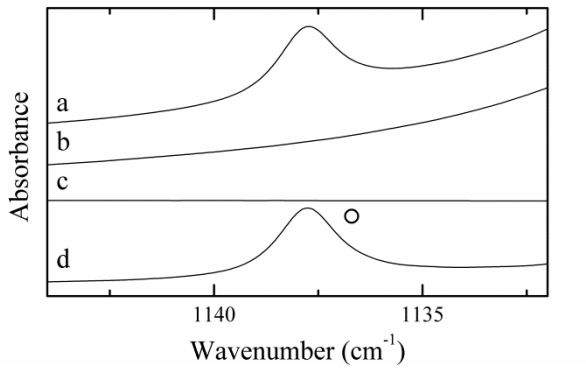

Figure 5: Infrared spectrum of the spectral region of the ν_3 mode of TMA-d_9 for mixtures of CHF_2Br with TMA-d_9 dissolved in LKr at 120 K. Trace *a* represents the mixed solution, while traces *b* and *c* show the rescaled spectra of the solutions containing only CHF_2Br or TMA-d_9, respectively. Trace *d* represents the spectrum of the complex which is obtained by subtracting the rescaled traces *b* and *c* from trace *a*. The complex band due to the hydrogen-bonded complex observed in trace *d* is marked with an open circle (°). Estimated mole fractions of the solution of the mixture are 2.3×10^{-3} for CHF_2Br and 1.5×10^{-3} for TMA-d_9.

Table 3: Experimental vibrational frequencies for the monomers and complex, experimental complexation shifts ($\Delta\nu_{exp,HB}$) and MP2/aug-cc-pVDZ-PP calculated complexation shifts, in cm^{-1}, for the hydrogen-bonded complex ($\Delta\nu_{calc,HB}$) and halogen-bonded complex ($\Delta\nu_{calc,XB}$) of CHF_2Br with TMA-d_9 dissolved in LKr at 120 K.

	Assignment	$\nu_{monomer}$	$\nu_{complex}$	$\Delta\nu_{exp}$	$\Delta\nu_{calc,HB}$	$\Delta\nu_{calc,XB}$
CHF_2Br		3025.4	-			
	ν_1	3014.4	2971.7	-42.7	-74.3	-12.1
	ν_7	1343.6	1378.0	34.4	60.2	-2.5
	ν_2	1277.8	1311.0	33.2	43.3	-5.6 [a]
	ν_8	1119.7	1107.7	-12.0	-11.8	-19.3
	ν_3	1093.5	1081.0	-12.5	-14.3	-5.6
	ν_4	712.9	704.5	-8.4	-8.2	0.1
	ν_5	578.0	576.8	-1.2	-0.8	-4.9
TMA-d_9	ν_{12}	2233.0	2235.3	2.3	1.1	0.2
	ν_1	2182.2	2187.9	5.7	3.3	5.5
	ν_{13}	2182.2	2187.9	5.7	3.9	5.8
	ν_2	2029.5	2030.0	0.5	9.9	7.1
	ν_{14}	2029.5	2038.6	9.1	11.3	7.9
	$\nu_{19}+\nu_{21}$	1226.5	1224.7	-1.8	-1.8	-0.8
	ν_{15}	1220.8	1224.7	3.9	-8.5	-1.1
	ν_3	1139.4 [b]	1137.8	-1.6	-2.2	-1.6
	ν_4	1063.0	1063.6	0.6	1.7	-1.3
	ν_{16}	1063.0	1063.6	0.6	0.2	-1.0
	ν_{17}	1055.7	-		0.7	0.4
	ν_{18}	1047.7	-		0.6	-0.7
	ν_5	1004.0	1014.0	10.0	10.3	6.0
	ν_{19}	873.9	873.5	-0.4	-0.6	0.1
	ν_{20}	832.8	-		-0.7	-1.0
	ν_6	741.1	739.6	-1.5	-2.5	-2.4

[a] mode is degenerate with TMA-d_9 modes in the *ab initio* calculations

[b] frequency obtained from a Raman measurement at 120 K

3.2.3 van 't Hoff Plots and experimental complexation enthalpies

Van 't Hoff plots based on measurements in the 120 - 156 K temperature interval of CHF_2Br·TMA(-d_9) mixtures, for which details are given in Table S5 of the ESI, yielded twelve experimental complexation enthalpies with an average value of -14.2(4) kJ mol^{-1}. An illustration of one of these van 't Hoff plots is given in Figure 6. For all Van 't Hoff plots derived, an *a posteriori* approach [21] correcting the slope of the regression lines obtained was used to correct the complexation enthalpy derived for thermal expansion of the solvent.[22]

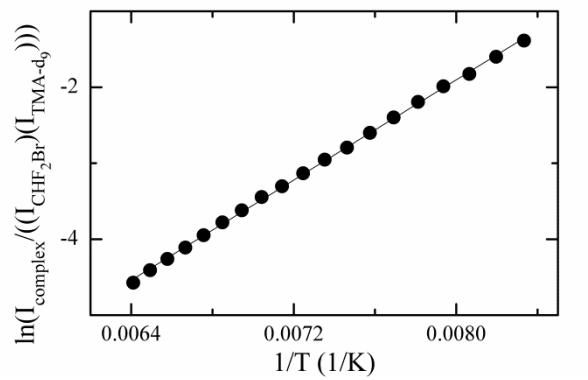

Figure 6: van 't Hoff plot of the hydrogen-bonded complex between CHF_2Br and TMA-d_9 in LKr in the 120-156 K temperature interval.

4. Discussion

For the mixtures involving CHF_2Br and TMA, all observed complex bands were assigned to the hydrogen-bonded complex, whereas no evidence for the presence of halogen-bonded complex was observed. Furthermore, an average experimental complexation enthalpy of -14.2(4) kJ mol^{-1} was determined from van 't Hoff plots for the hydrogen-bonded complex, which is in good agreement with the calculated value of -16.5 kJ mol^{-1}. Comparison with the *ab initio* results of the CHF_2I·TMA complexes [18] also reveals that the transition from iodine to bromine strongly decreases the strength of the halogen-bonded complex, the calculated complexation enthalpies being -23.4 kJ mol^{-1} and -13.6 kJ mol^{-1}. For the hydrogen-bonded complexes, nearly identical calculated complexation enthalpies are computed, amounting to -16.6 kJ mol^{-1} for the CHF_2I·TMA hydrogen-bonded complex and -16.5 kJ mol^{-1} for the CHF_2Br·TMA hydrogen-bonded complex, thus demonstrating that the nature of the heavier halogen present in the molecule has very little effect on the hydrogen-bonded complex. The negligible influence of this halogen atom on the hydrogen bond strength is also confirmed experimentally, where the observed complexation enthalpy of -14.2(4) kJ mol^{-1} for the hydrogen-bonded complex between CHF_2Br and TMA is nearly identical to the complexation enthalpy of -14.7(2) kJ mol^{-1} for the hydrogen-bonded complex between CHF_2I and TMA. Furthermore, these values are also very comparable to the complexation enthalpy of -14.6(8) kJ mol^{-1} reported for the complex between TMA and fluoroform (CF_3H) in liquid argon and liquid krypton by Bertsev et al. [33] and by Hauchecorne et al. [34], thus confirming that the exact nature of the third halogen atom in CHF_2X molecules does not influence the strength of the hydrogen-bonded complex with TMA noticeably.

Also worth noting is the fact that the halogen-bonded complex between bromotrifluoromethane (CF_3Br) and TMA, reported previously with a complexation enthalpy in liquid argon of -18.3(1) kJ mol^{-1} [34], is noticeably stronger than the hydrogen-bonded complex with fluoroform. Comparison with the results of the current study show that replacing one of the fluorine atoms of CF_3Br with a hydrogen

atom reduced the potential strength of the bromine halogen bond sufficiently for it no longer being able to compete with the hydrogen bond.

Even though the absence of the halogen-bonded complex comes as a bit of a surprise considering its calculated enthalpy in solution is only 2.9 kJ mol^{-1} higher than that of the hydrogen-bonded complex, which corresponds with a relative population estimated to be in the order of 5 to 10 % at 138 K, it is consistent with observations in a previous study involving halothane (1-bromo-1-chloro-2,2,2-trifluoroethane) and TMA, where the halogen-bonded complex was also not observed. [35] the reason for this, most probably, is related to the fact that in both halothane and CHF_2Br, the bromine and hydrogen atom are covalently bonded to the same carbon atom, along with two electron withdrawing groups (i.e. a chlorine atom and trifluoromethyl group for halothane). The absence of halogen-bonded complex for both donor molecules in mixtures containing TMA, a Lewis base that has proven to be an excellent target for halogen bonding in previous studies, [18, 20] is a good indicator for the fact that bromine halogen bonding is significantly weaker than hydrogen bonding when both donor atoms are covalently bonded to the same carbon atom. It would therefore be interesting to see whether this tendency holds up when both donor atoms are covalently bonded to different carbon atoms in larger molecules, such as 1-bromo-1,2,2-trifluoroethane or 1-bromo-2,3,5,6-tetrafluorobenzene. *Ab initio* calculations at the MP2/aug-cc-pVDZ-PP level of theory yielded complexation energies of -24.9 kJ mol^{-1} for the HB complex and -23.2 kJ mol^{-1} for the XB complex with the former donor and -22.3 kJ mol^{-1} for the HB complex and -25.1 kJ mol^{-1} for the XB complex with the latter donor.

The absence of the halogen-bonded complex has also been observed in a preliminary study by Delanoye et al. [36] investigating mixtures of CHF_2Br with dimethyl ether, acetone or oxirane in liquid krypton. Furthermore, with an experimental complexation enthalpy in LKr of -12.0(1) kJ mol^{-1}, the CHF_2Br·DME hydrogen-bonded complex is weaker than the currently studied hydrogen-bonded complex with TMA ($\Delta H°$(LKr) = -14.2(4) kJ mol^{-1}). This tendency has also been observed in the study of the complexes with CHF_2I [18], where the hydrogen-bonded complexes with DME and TMA had experimental complexation enthalpies of -10.5(5) kJ mol^{-1} and -14.7(2) kJ mol^{-1} respectively and the study with the bond donor molecule CH_2FI [20], with complexation enthalpies of -7.0(2) kJ mol^{-1} for the HB complex with DME and -9.6(2) kJ mol^{-1} for the HB complex with TMA.

5. Conclusions

Ab initio calculations yielded both a stable hydrogen-bonded an halogen-bonded complex between CHF_2Br and TMA($-d_9$), the complexation enthalpies in liquid krypton being -16.5 and -13.6 kJ mol^{-1} respectively, upon correction for thermal and solvent effects on the complexation energies of CCSD(T)/CBS quality. Infrared spectroscopy on mixtures of both compounds in LKr revealed that

only hydrogen-bonded complex is present, for which an experimental complexation enthalpy was determined of -14.2(4) kJ mol^{-1}. Comparison with the complexes of CHF_2I with TMA shows that the transition from iodine to bromine greatly diminishes the strength of the halogen-bonded complex, as expected for smaller halogen atoms, while the influence on the strength of the hydrogen-bonded complex is negligible.

Supporting Information Available:

MP2/aug-cc-pVDZ(-PP) cartesian coordinates, vibrational frequencies, IR and Raman intensities of CHF_2Br, TMA and the halogen and hydrogen-bonded complexes and overview of parameters used in van 't Hoff plots.

Acknowledgements

Y.G. wishes to thank the FWO-Vlaanderen for a doctoral fellowship (11O9516N). W.H. acknowledges financial support through FWO-Vlaanderen and the Special Research Fund BOF (UA). F.D.P. wishes to acknowledge FWO-Vlaanderen and the Free University of Brussels (VUB) for continuous support to the ALGC research group, in particular the VUB for a Strategic Research Program awarded to ALGC, started up at January 1, 2013. The Hercules foundation and the VSC are thanked for generously providing the required CPU resources.

Graphical abstract for Table of contents:

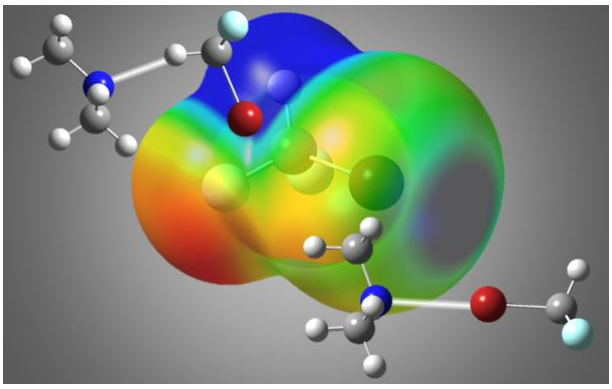

References:

1 P. Politzer, P. Lane, M. C. Concha, Y. Ma, J. S. Murray, *J. Mol. Model.,* 2007, ***13***, 305-311, 10.1007/s00894-006-0154-7.
2 P. Politzer, J. S. Murray, *ChemPhysChem,* 2013, ***14***, 278-294, 10.1002/cphc.201200799.
3 P. Metrangolo, G. Resnati, *Cryst. Growth Des.,* 2012, ***12***, 5835-5838, 10.1021/cg301427a.
4 A. C. Legon, *Phys. Chem. Chem. Phys.,* 2010, ***12***, 7736-7747, 10.1039/c002129f.

5 T. Clark, M. Hennemann, J. S. Murray, P. Politzer, *J. Mol. Model.,* 2007, ***13***, 291-296, 10.1007/s00894-006-0130-2.
6 K. E. Riley, J. S. Murray, J. Fanfrlik, J. Rezac, R. J. Sola, M. C. Concha, F. M. Ramos, P. Politzer, *J. Mol. Model.,* 2011, ***17***, 3309-3318, 10.1007/s00894-011-1015-6.
7 P. Metrangolo, G. Resnati, T. Pilati, S. Biella, *Struct. Bond.,* 2008, ***126***, 105-136, 10.1007/430_2007_060.
8 P. Metrangolo, G. Resnati, *Science,* 2008, ***321***, 918-919, 10.1126/science.1162215.
9 S. Zhu, C. Xing, W. Xu, Z. Li, *Tetrahedron Lett.,* 2004, ***45***, 777-780, 10.1016/j.tetlet.2003.11.100.
10 J. Marti-Rujas, L. Colombo, J. Lu, A. Dey, G. Terraneo, P. Metrangolo, T. Pilati, G. Resnati, *Chem. Commun.,* 2012, ***48***, 8207-8209, 10.1039/c2cc33682k.
11 A. R. Voth, P. Khuu, K. Oishi, P. S. Ho, *Nat. Chem.,* 2009, ***1***, 74-79, 10.1038/nchem.112.
12 B. Jing, Q. Li, R. Li, B. Gong, Z. Liu, W. Li, J. Cheng, J. Sun, *Comput. Theor. Chem.,* 2011, ***963***, 417-421, 10.1016/j.comptc.2010.11.006.
13 C. B. Aakeröy, M. Fasulo, N. Schultheiss, J. Desper, C. Moore, *J. Am. Chem. Soc.,* 2007, ***129***, 13772-13773, 10.1021/ja073201c.
14 C. B. Aakeröy, S. Panikkattu, P. D. Chopade, J. Desper, *CrystEngComm,* 2013, ***15***, 3125-3136, 10.1039/c2ce26747k.
15 C. B. Aakeröy, C. L. Spartz, S. Dembowski, S. Dwyre, J. Desper, *IUCrJ,* 2015, ***2***, 498-510, 10.1107/s2052252515010854.
16 P. Politzer, J. S. Murray, P. Lane, *Int. J. Quantum Chem.,* 2007, ***107***, 3046-3052, 10.1002/qua.21419.
17 T. Shirman, M. Boterashvili, M. Orbach, D. Freeman, L. J. W. Shimon, M. Lahav, M. E. van der Boom, *Cryst. Growth Des.,* 2015, ***15***, 4756-4759, 10.1021/acs.cgd.5b01260.
18 N. Nagels, Y. Geboes, B. Pinter, F. De Proft, W. A. Herrebout, *Chem. - Eur. J.,* 2014, ***20***, 8433-8443, 10.1002/chem.201402116.
19 Y. Geboes, F. De Proft, W. A. Herrebout, *Acta Cryst.,* 2017, 168-178, 10.1107/S2052520617001354.
20 Y. Geboes, F. De Proft, W. A. Herrebout, *J. Phys. Chem. A,* 2017, ***121***, 4180-4188, 10.1021/acs.jpca.7b03206.
21 W. A. Herrebout, *Top. Curr. Chem.,* 2015, ***358***, 79-154, 10.1007/128_2014_559.
22 B. J. van der Veken, *J. Phys. Chem.,* 1996, ***100***, 17436-17438, 10.1021/jp9617478.
23 M. J. Frisch, G. W. Trucks, H. B. Schlegel, G. E. Scuseria, M. A. Robb, J. R. Cheeseman, G. Scalmani, V. Barone, B. Mennucci, G. A. Petersson, H. Nakatsuji, M. Caricato, X. Li, H. P. Hratchian, A. F. Izmaylov, J. Bloino, G. Zheng, J. L. Sonnenberg, M. Hada, M. Ehara, K. Toyota, R. Fukuda, J. Hasegawa, M. Ishida, T. Nakajima, Y. Honda, O. Kitao, H. Nakai, T. Vreven, J. A. Montgomery, Jr., J. E. Peralta, F. Ogliaro, M. Bearpark, J. J. Heyd, E. Brothers, K. N. Kudin, V. N. Staroverov, R. Kobayashi, J. Normand, K. Raghavachari, A. Rendell, J. C. Burant, S. S. Iyengar, J. Tomasi, M. Cossi, N. Rega, N. J. Millam, M. Klene, J. E. Knox, J. B. Cross, V. Bakken, C. Adamo, J. Jaramillo, R. Gomperts, R. E. Stratmann, O. Yazyev, A. J. Austin, R. Cammi, C. Pomelli, J. W. Ochterski, R. L. Martin, K. Morokuma, V. G. Zakrzewski, G. A. Voth, P. Salvador, J. J. Dannenberg, S. Dapprich, A. D. Daniels, Ö. Farkas, J. B. Foresman, J. V. Ortiz, J. Cioslowski, D. J. Fox, *Gaussian 09, Revision D.01*, Wallingford, CT, USA, 2009.
24 D. Feller, *J. Comput. Chem.,* 1996, ***17***, 1571-1586, 10.1002/(SICI)1096-987X(199610)17:13<1571::AID-JCC9>3.0.CO;2-P.
25 K. L. Schuchardt, B. T. Didier, T. Elsethagen, L. Sun, V. Gurumoorthi, J. Chase, J. Li, T. L. Windus, *J. Chem. Inf. Model.,* 2007, ***47***, 1045-1052, 10.1021/ci600510j.
26 S. F. Boys, F. Bernardi, *Mol. Phys.,* 1970, ***19***, 553-566, 10.1080/00268977000101561.
27 H.-J. Werner, P. J. Knowles, G. Knizia, F. R. Manby, M. Schütz, P. Celani, T. Korona, R. Lindh, A. Mitrushenkov, G. Rauhut, K. R. Shamasundar, T. B. Adler, R. D. Amos, A. Bernhardsson, A. Berning, D. L. Cooper, M. J. O. Deegan, A. J. Dobbyn, F. Eckert, E. Goll, C. Hampel, A. Hesselmann, G. Hetzer, T. Hrenar, G. Jansen, C. Köppl, Y. Liu, A. W. Lloyd, R. A. Mata, A. J.

May, S. J. McNicholas, W. Meyer, M. E. Mura, A. Nicklass, D. O'Neill, P. Palmieri, D. Peng, K. Pflüger, R. Pitzer, M. Reiher, T. Shiozaki, H. Stoll, A. J. Stone, R. Tarroni, T. Thorsteinsson, M. Wang, *MOLPRO, version 2012.1, A Package of Ab Initio Programs*, 2012.

28 D. G. Truhlar, *Chem. Phys. Lett.,* 1998, ***294***, 45-48, 10.1016/s0009-2614(98)00866-5.

29 P. Jurečka, P. Hobza, *J. Am. Chem. Soc.,* 2003, ***125***, 15608-15613, 10.1021/ja036611j.

30 W. L. Jorgensen, *BOSS - Biochemical and Organic Simulation System*, John Wiley & Sons Ltd., New York, NY, USA, **1998**.

31 E. R. Johnson, S. Keinan, P. Mori-Sánchez, J. Contreras-García, A. J. Cohen, W. Yang, *J. Am. Chem. Soc.,* 2010, ***132***, 6498-6506, 10.1021/ja100936w.

32 J. Contreras-García, E. R. Johnson, S. Keinan, R. Chaudret, J.-P. Piquemal, D. N. Beratan, W. Yang, *J. Chem. Theory Comput.,* 2011, ***7***, 625-632, 10.1021/ct100641a.

33 V. V. Bertsev, N. S. Golubev, D. N. Shchepkin, *Opt. Spectrosc.,* 1976, ***40***, 543-544,

34 D. Hauchecorne, B. J. van der Veken, A. Moiana, W. A. Herrebout, *Chem. Phys.,* 2010, ***374***, 30-36, 10.1016/j.chemphys.2010.06.004.

35 B. Michielsen, W. A. Herrebout, *Molecular Interactions with Halothane: a Spectroscopic Study*, University of Antwerp (Antwerp, Belgium), **2011**. Unpublished Results

36 S. N. Delanoye, W. A. Herrebout, B. J. van der Veken, *Cryospectroscopic Study of Proper and Improper C-H···O Hydrogen Bonds: the van der Waals Complexes of Dimethyl Ether, Acetone and Oxirane with Diverse Proton Donors*, University of Antwerp **2004**. Unpublished Results